Title
Using distributed temperature sensing to detect CO2 leakage along the injection well casing

Authors
Zhang, Yingqi
Jung, Yoojin
Freifeld, Barry
et al.

Publication Date
2018-07-01

DOI
10.1016/j.ijggc.2018.04.011

Peer reviewed

Using distributed temperature sensing to detect CO_2 leakage along the injection well casing

Yingqi Zhang[a] Yoojin Jung[a] Barry Freifeld[a] Stefan Finsterle[ab]

Abstract

The objective of this study is to evaluate the sensitivity of Distributed Temperature Sensing (DTS) data to detect CO_2 leakage along an injection well casing. This paper describes the relationship between the CO_2 leakage rate and temperature response at DTS locations, and the method and numerical model used for understanding such a relationship. The uncertainties in the parameters are propagated to the interpretation of DTS measurements, which may lead to false positive and false negative identifications of CO_2 leakage. We propose to identify CO_2 leakage by analyzing both temperature history plots at selected vertical locations as well as the vertical temperature profiles at different times. The analysis should be combined with numerical simulations for the estimation of leakage rates. In addition, leakage needs to be confirmed by data from a warm-up test (temperature recovery after injection of cold CO_2 is stopped) to minimize the probability of false identifications.

Keywords: CO2 storage, Injection well casing leakage, Distributed temperature sensing (DTS), Leakage detection, Minimum detectable leakage rate

1. Introduction

One of the largest concerns in geologic CO_2 storage (GCS) projects is the potential escape of the injected CO_2 from the storage reservoir to regions with vulnerable resources (e.g., a drinking water aquifer) through various leakage pathways. There are two main leakage scenarios (Benson, 2006; Pruess, 2008; Bachu and Celia, 2009; Zhang et al., 2010): (1) leakage through a well, either the injection well itself, or a nearby well that is improperly sealed, and (2) leakage through subvertical faults or fracture zones intersecting the caprock. Leakage may not only constitute a safety hazard, but also reduces the effectiveness of a GCS project. To address leakage concerns, it is necessary to (1) improve our understanding of the development of potential leakage and CO_2 migration pathways, (2) develop monitoring techniques for leakage detection, and (3) propose methods for leakage control (Zahasky and Benson, 2014).

The focus of this study is to detect potential CO_2 leakage along the casing of an injection well. If an injection well has either mechanical defects developed during well construction, or experienced chemical degradation of well cements during and after operation, CO_2 may travel upwards along the outside of the well casing until it encounters a highly permeable thief zone or the end of the defect. It may flow all the way to the vulnerable resource or land surface. Compared to the other types of leakage, the leakage flux along

a well is relatively high but may pose only a local risk (Benson, 2006). Prior investigations of the potential leakage due to well integrity issues include (1) laboratory or field experiments (e.g., Kutchko et al., 2007; Carey et al., 2010; Crow et al., 2010; Duguid et al., 2011), where the main purpose is to examine the degradation of cement exposed to CO_2 or brine; (2) analyses of well data (e.g., Watson and Bachu, 2009) or literature review (e.g., Zhang and Bachu, 2011), with the purpose to identify major factors contributing to wellbore leakage, e.g., low cement top or exposed casing; and (3) numerical simulations (e.g., Nordbotten et al., 2005; Gasda et al., 2008, Gasda et al., 2013; Crow et al., 2010; Celia et al., 2011), with the focus either on tool development for understanding leakage processes (Nordbotten et al., 2005, Nordbotten et al., 2009) or experimental design to estimate leaky well properties (Gasda et al., 2008, Gasda et al., 2013; Nogues et al., 2011; Duguid et al., 2013). Gasda et al. (2008) propose to estimate leaky well permeability using a vertical interference test in which packers are used to isolate two well sections at different elevations, and the pressure response due to fluid leakage from one section to the other is used to infer an effective permeability of the leakage pathway. For detection of leaky wells, Nogues et al. (2012) propose to analyze pressure data recorded at monitoring wells in the formation above the reservoir to detect leakage through abandoned wells. They state that leakage can be detected if the pressure perturbation induced by leakage flow is larger than the pressure gauge accuracy. Duguid et al. (2013) propose to collect pre-injection pressure data to be used as a baseline for leakage detection. Thermal logging (Zeng et al., 2012) has been proposed for leakage detection. Their study focused on how temperature may change along the leakage pathway using a 1D model, assuming that CO_2 never leaks laterally into the formation. In addition, using thermal logging requires upfront knowledge whether leakage has occurred or monitoring is done on a discrete basis, which means leakage may not be detected in a timely manner as thermal logging does not take continuous measurements over time. Zeidouni et al. (2014)investigated above-zone temperature variations associated with leakage of CO_2 and brine from a storage reservoir. They concluded that temperature data will be most useful if collected along potentially leaky wells and/or wells intersecting potentially leaky faults. In addition, Mao et al. (2017) discussed how flow properties of the leakage pathway affect thermal signals caused by the leaking CO_2. The conclusion from the leaky well scenario is that pressure drop and leakage flux are two controlling factors.

In this work, we propose to use temperature data collected by a distributed temperature sensing (DTS) system in the injection well for real-time leakage detection along the well casing. A notable difference between leakage through injection wells and other leaky wells (abandoned or monitoring wells) is that the temperature of CO_2 leaking from an injection well depends much more on the injected CO_2 temperature, whereas in other cases, CO_2 has been mixed with reservoir fluid. In a DTS system, temperatures are

recorded continuously along an optical sensor cable, resulting in data with high spatial and temporal resolution along the entire profile. DTS is relatively easy to install and has a long life-span. The advantage of using temperature data for monitoring is that it is highly accurate with a measurement error of about 0.1 °C (Paterson et al., 2011) and relatively inexpensive.

When injecting CO_2, two thermal processes affect temperature and thus make DTS measurements suitable for monitoring CO_2 migration. First, convective heat transfer leads to a temperature change, as CO_2 or brine replacing the resident pore fluid is likely to have a different temperature than the local environment. Second, conductive heat transfer also leads to a temperature change because the lower thermal diffusivity CO_2 has compared to brine or drilling fluid will perturb ongoing heat transfer processes. Installing a DTS system inside the injection well (behind the well casing) to monitor CO_2 injection can help us understand the thermodynamics in a wellbore (Wiese, 2014) and detect leakage along the well casing. DTS systems have been installed in three CO_2 storage projects: The injection well at Ketzin, Germany (Liebscher et al., 2013; Wiese, 2014), monitoring wells at Cranfield, Mississippi, USA (Núñez-López, 2011; Doughty and Freifeld, 2013) and Ketzin (Henninges, 2010), and the injection well coupled with a heater at Otway, Australia (Zhang et al., 2011).

The objective of this study is to evaluate the sensitivity of DTS data for the detection of CO_2leakage along an injection well casing. We try to identify the minimum leakage rate that can be detected by the temperature signals measured by DTS. To achieve this objective, we first establish a relationship between the leakage rate and the DTS temperature signal measured behind the injection well casing. We also investigate how parameter uncertainty affects this signal. Finally, we examine the conditions for false leakage identification. While the well and formation properties (e.g., permeability of the leakage pathway, reservoir and thief zone) affect leakage, it is not the purpose of this study to infer those properties. As the first step for leakage detection, our goal is to identify the minimum leakage rate detectable by DTS. Estimating properties of the leakage pathway based on DTS measurements will be addressed in future research.

The remainder of the paper is organized as follows: Section 2 is a brief description of the site and system setup, while Section 3 describes the numerical model and its assumptions. In Section 4, we focus on the identification of the minimum detectable leakage rate. Section 5provides a summary and conclusions.

2. Geological conditions and system setup

The analysis is conducted for a synthetic carbon storage site. However, the field conditions and well setup are taken from an actual site to ensure that the details of the well completion and injection operations are realistic and consistent with industry practice. For the geological conditions at the storage site, the following assumptions are made: (1) The storage reservoir is a 50 m

thick sandstone located at 2 km depth; (2) there are three seal layers above the storage reservoir (referred to in ascending order as Seal1, Seal2, and Seal3), which are supposed to trap the injected CO_2; (3) Seal3 is 1700 m beneath the ground surface; and (4) the storage site is located in a cold region and the temperature of the injected CO_2 is about −4 °C. The schematic of the injection well and its DTS configuration as well as geological layers used in the numerical model are shown in Fig. 1. The DTS is installed on the outside of a cemented 7″ production casing. The lower end of the DTS is in the Seal1 layer, about 88 m above the top of the storage reservoir. The reason for not extending the DTS cable further down is to eliminate the risk that corrosion of the cable from a mixture of CO_2 and water will compromise the integrity on the entire injection well. CO_2 is injected through the 3 1/2″ tubing and into the storage reservoir via perforations in the 7″ casing. The annular space between the injection tubing and the casing is filled with inert fluid. A packer prevents dense phase CO_2 from flowing back up through the casing, which has been pressure tested to ensure its sealing capacity.

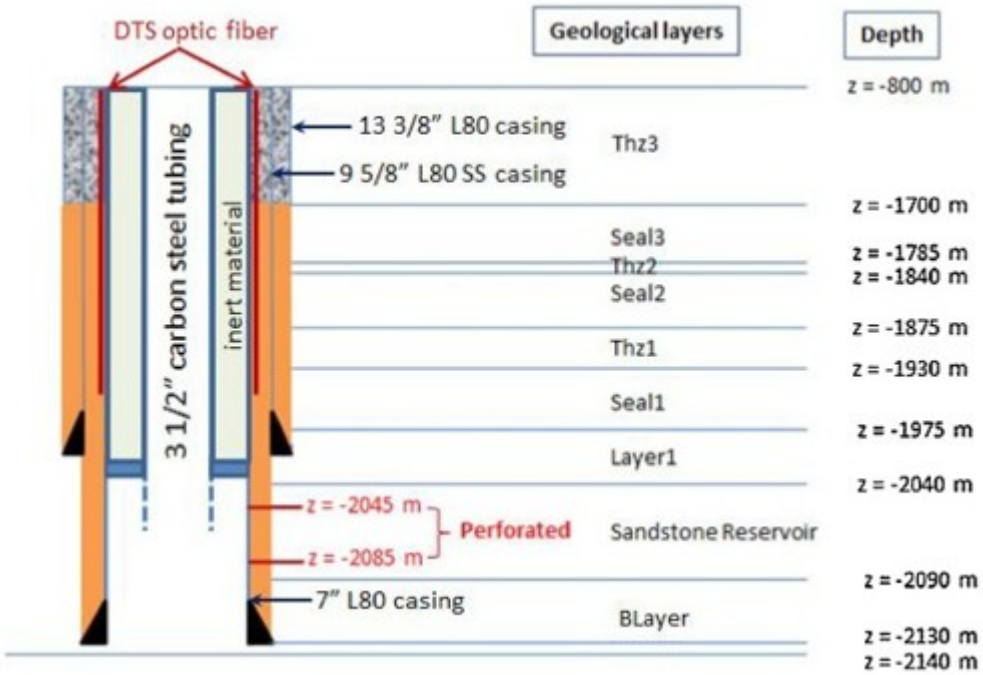

Fig. 1. Schematic of the injection well and geological layers. The right side shows the formation names and depths used in the numerical model. The color change in cement indicates cement below and above the top seal layer (Seal3).

The scenario of concern consists of a leakage pathway along the cement outside the API 9 5/8″ L80 SS casing (see Fig. 1), in which case CO_2 may leak out from the storage reservoir and through Layer 1, and then go into one of the thief zones above (e.g., thief zones Thz 1–3, which have a relatively high permeability). The injected CO_2 has a much lower temperature at the ground surface than the reservoir temperature. We assume the initial temperature profile of the formation and wellbore follows the geothermal gradient. During CO_2 injection, the formation around the wellbore gradually cools down due to

conductive heat transfer between the formation and the flowing wellbore. If some of the injected cold CO_2 starts to leak and flow along the wellbore casing, the cement gets even colder due to convective heat transfer, which will also affect the cement temperature inside the 9 5/8″ casing due to heat conduction. If the leakage rate is high enough to create a detectable temperature signal at locations where DTS measurements are placed, one may conclude that CO_2 is leaking along the well casing, suggesting that further investigations are required.

3. Models, tools and assumptions

Three pieces of software are used to conduct the analysis described in this paper. TOUGH2 (Pruess et al., 2011; Finsterle et al., 2008), a numerical simulator for non-isothermal multiphase flow, with the ECO2N (Pruess and Spycher, 2007) fluid property module, which is designed for applications involving geologic storage of supercritical CO_2 in saline aquifers, is used to simulate the physical process of CO_2 injection, associated cooling, as well as the warm-up process after injection. It includes a comprehensive description of the thermodynamics and thermophysical properties of H_2O – NaCl -CO_2 mixtures, that reproduces fluid properties largely within experimental error for the temperature, pressure and salinity conditions of interest ($10\,°C \leq T \leq 110\,°C$; $P \leq 600$ bar; salinity up to full halite saturation). Water properties in TOUGH2/ECO2N are calculated from the steam table equations as given by the International Formulation Committee (1967). Properties of pure CO_2 are obtained from correlations developed by Altunin (1975), which were found to be very accurate (Garcia, 2003). iTOUGH2 (Finsterle, 2004), a simulation-optimization framework that provides inverse modeling capabilities (including uncertainty quantification) for the TOUGH2 code, is used to establish the relationship between leakage rate and temperature signal, identify the minimum detectable leakage rate and examine how uncertainty affects this minimum rate. T2Well (Pan and Oldenburg, 2014) is a software package that incorporates an accurate description of wellbore processes coupled with TOUGH2. To simulate flow in an open well, we estimate an effective wellbore permeability by fitting the flow and pressure at the bottom of the well calculated by TOUGH2 using Darcy’s Law to those calculated by T2Well using a multi-phase drift-flux model. In later simulations, this effective permeability is used in the main TOUGH2-ECO2N simulations (without T2Well) to model the thermodynamics and pressure inside and around the wellbore. This approach is used only for simulating CO_2 injection through the open wellbore, but not for CO_2 leakage through the porous cement.

DTS data are analyzed using a 2D axisymmetric heat and mass transport model, which has a radial extent of 1500 m. The radial discretization at the wellbore honors the radii and wall thickness of the tubing, casing and annular space (see Table 1). The mesh for the formation is relatively fine adjacent to the wellbore to make sure the temperature and pressure around the wellbore is modeled accurately, i.e., starting at 0.01 m next to the well,

with gradually increasing element sizes up to the outer boundary. The model extends vertically from the bottom layer (BLayer) at 2140 m–800 m depth (the reason for this depth will be given below). Vertical discretization is typically 10 m. Pressure and temperature are held constant at the outer boundary. No flow boundary conditions are applied at the top and bottom of the model domain. The leakage pathway is represented by a damaged cement column with larger permeability outside the API 9 5/8″ casing (i.e., it is not modeled explicitly using a gap). The use of a 2D radial model assumes the cement outside the casing is homogeneously degraded (i.e., the leakage pathway is ring-shaped). The completion fluid in the annulus between the 3 ½″ tubing and the API 7″ casing (see Fig. 1) is sealed at the bottom by a packer and at the top by the wellhead and thus is hydraulically isolated from the system, but allows for heat conduction. Before CO_2 is injected, the formation is saturated with brine with a hydrostatic pressure profile. The temperature profile is established based on an average surface temperature of 2 °C and a geothermal gradient of 0.023 °C/m. In our scenario the temperature of injected CO_2 at the wellhead is −4 °C, while the minimum temperature that can be handled by TOUGH2-ECO2N is 3.1 °C (this is the minimum temperature in the lookup table for calculating CO_2 properties, while the 10 °C stated previously is the lower bound of temperature that reproduces fluid properties largely within experimental error). We performed an initial simulation in which we elevated the temperature of both injected $CO_2$and surrounding formation (from surface to target reservoir) by 8 °C to quantify the heat transfer occurring while the CO_2 travels down the tubing starting at the ground surface. This numerical evaluation indicates that the injected CO_2 is heated up to +4 °C at approximately 800 m depth after a short period of injection. Using the thermal conditions suggested by these initial simulation results, we simplified our model to only include the formation below a depth of 800 m, as shown in Fig. 1. We assume the injected CO_2 at 800 m depth is 4 °C, whereas the formation temperature is about 20 °C. For a real application the temperature at any depth depends on surface temperature, injected CO_2 temperature, the injection rate, injection duration, and the thermal properties of the borehole environment and formation. Using a constant 4 °C injection temperature at 800 m depth serves as an initial assumption used in our simulations. The effect of this assumption will be discussed in a later section.

Table 1. Tubing and casing size of the injection well.

	Tubing	7″ L80 casing	9 5/8″ L80 SS casing	13 3/8″ L80 SS casing
Diameter (inch)	3.5	7	9.625	13.375
Wall thickness (inch)	0.254	0.362	0.395	0.514

A constant wellhead pressure is used for the simulation, leading to a CO_2 injection rate between 12.8 and 13.0 kg/s (~0.4 million tons per year). The leakage rate of CO_2 is defined as the flow rate of CO_2 along the cement outside the 9 5/8″ L80 SS casing at the elevation of the first seal layer, Seal1. This rate is mainly controlled by the contrast between the permeability of the leakage pathway and the permeability of the storage reservoir. The key hydrologic and thermal parameters used in the base-case scenario are listed in Table 2. Three assumptions are made for the base case scenario:

1. CO_2 leakage starts after 50 days of CO_2 injection.

2. The first thief zone encountered by CO_2 leaking along the injection well is layer Thz1.

3. The leakage pathway ends at a depth of 1500 m.

Table 2. Key hydrologic and thermal parameters used in the base-case scenario simulation.

Property	Geological layer	Value
Permeability (m^2)	reservoir	5.e-13
	Layer1	5.e-15
	Seal1	1.e-18
	Thz1, Thz2	1.e-12
	Seal2, Seal3	2.e-20
	4 sublayers of Thz3	1.e-17–1.e-14
	damaged cement	1.6e-10
Porosity	reservoir	0.2
	Thief zones	0.15
	Seal2, Seal3	5.5
Thermal conductivity wet (W/m °C)	Other geological layers	3.0
	Cement	2.0
	Inert material	0.1
Thermal conductivity dry (W/m °C)	Seal2, Seal3	4.5
	Other geological layers	1.5

Property	Geological layer	Value
Heat capacity (J/kg °C)	Cement	1.0
	Tubing	500.
	Inert material	1900.
	Cement	920.
	Geological formation	1000.

The effects of these base-case assumptions will be addressed in later sections.

4. Identification of minimum detectable leakage rate

In this section, we examine a base case scenario, where we compare the vertical temperature profiles at location of DTS cables (outside the 7″ casing) for two cases: The first case serves as a reference case (Ref-case), in which there is no leakage of CO_2. In the second case, some of the injected CO_2 leaks out of the storage reservoir through the cement outside the 9 5/8″ L80 SS casing (Leak-case). Next, we identify the minimum leakage rate for this particular scenario, without consideration of uncertainty in the input parameters. Finally, we analyze a variety of different scenarios, including: 1) varying assumptions/setups used in the base case scenario (geological setting, leakage timing and end location of leakage pathway); 2) adding fluctuations in the operating conditions; 3) changing tempearture in the injected CO_2; and 4) considering uncertainty in the input parameters. The goal is to investigate how leakage identification will be affected if the actual scenario deviates from the base case scenario, and to examine the potential for false leakage detection.

4.1. Base case scenario

For the base case scenario, we simulate the CO_2 injection for 110 days, followed by 10 days of post-injection observation, a total of 120 days. Using numerical simulations we obtain the temperatures at DTS measurement locations and compare them between the Ref-case and the Leak-case. The leakage rate during the injection period (i.e., from day 50 to day 110) is about 0.09 kg/s, approximately 0.7% of the injection rate.

Fig. 2 shows the vertical temperature profiles along the DTS cable over time for both Ref-case and Leak-case. The temperature profile labeled as 0d shows the initial temperature in the well casing, which is also the formation temperature following the geothermal gradient. The temperature at the storage reservoir is about 50 °C. During CO_2 injection, the temperature in the well casing cools down by the cold injected CO_2 because the completion fluid between the tubing and casing is thermally conductive. As the thermal gradient between the injected fluid and the surrounding well is greatest upon initiation of injection, the temperature drop in the well casing is much more pronounced during the initial injection period (i.e., ~3 °C temperature drop for the first day) than later time, when it gradually reaches near steady-state conditions (i.e., ~total of 6 °C drop for 50 days). Similarly, the temperature increase is greater during the first day of the post-injection than at later times. At 50 days, CO_2 temperature at the location where it enters the storage reservoir is about 13 °C and pressure is about 21 MPa. For Ref-case, without any leakage the temperature profiles along the well casing at different times are seen to be offset roughly parallel to each other, indicating that the changes are proportional to the induced temperature gradient between the injected fluid and the formation temperature. This implies that

heat transfer between well casing and formation is controlled by conduction and not affected by advection.

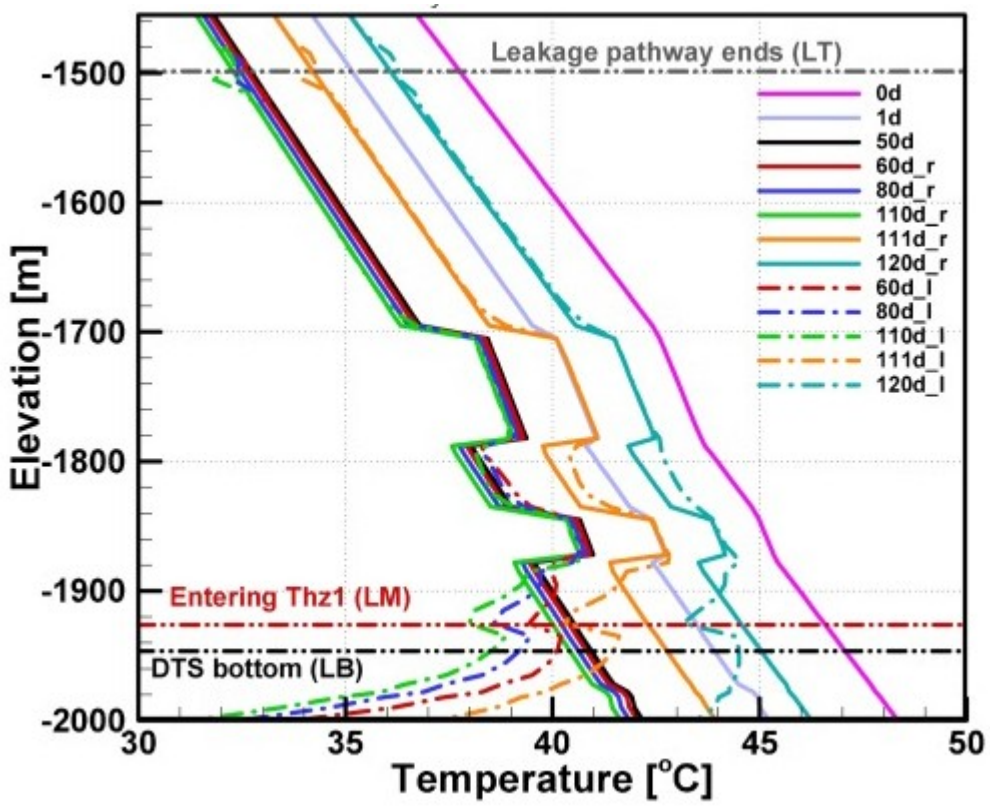

Fig. 2. Temperature profiles at different times during and post injection for the base case scenario. For the legend: 0d – beginning of injection; 1d – 1 days after injection; 50d – 50 days after injection when leakage starts; 60d – 60 days after injection, 10 days after leakage starts; 80d – 80 days after injection, 30 days after leakage starts; 110d – 110 days after injection, 60 days after leakage starts; 111d – 111 days since injection starts, 1 days after injection stops; 120d – 120 days since injection starts, 10 days after injection stops. The temperature profiles for the first 50 days are the same for Ref-case and Leak-case. For temperature profiles after 50 days, "_r" represents Ref-case (i.e., no leakage), shown in solid lines; "_l" represents Leak-case, shown in dashed-dotted lines. The legend is the same for other profile figures.

For Leak-case, a leakage pathway is assumed, starting from the storage reservoir where CO_2 enters, through Layer 1 (under the cement outside the 9 5/8″ L80 SS casing), and into the bad cement outside the 9 5/8″ L80 SS casing. This is a model simplification of a more realistic, uncertain leakage pathway. After the 13 °C CO_2 enters the storage reservoir, some of it may escape from the reservoir and finds its way through Layer1 and into the degraded cement next to the well casing. There is no water entering the thief zone. For this case, three observations are made: (1) a distinct cooling trend at the lower end of the DTS, indicating the existence of a cold source, attributed to cold CO_2 leaked from the storage reservoir; (2) a strong temperature depression at elevation −1925 m, indicating that escaped CO_2 enters the thief zone (Thz1) at this depth; and (3) another temperature depression at elevation −1500 m, indicating that escaped CO_2 accumulates at the end of the leakage pathway. $CO_2$is able to spread laterally because we

assume the degraded cement is hydraulically connected to the surrounding formation. To summarize, the temperature along the well casing is determined by the temperature of the injected CO_2 if there is no leakage through the well casing (thermal conduction between tubing and casing). By contrast, if leakage occurs, the temperature is determined by the superposition of heat transfer caused by CO_2flowing in the tubing and CO_2 leaking through degraded cement outside the casing. The temperature of the leaking CO_2 is affected not only by the heat exchange with its environment but also by Joule-Thomson effects, i.e., cooling due to the pressure drop as CO_2 travels up through the leakage pathway. Joule-Thomson effects are captured by the equation-of-state formulation used in TOUGH2-ECO2N. The Joule-Thomson coefficient varies depending on the temperature and pressure conditions. For Leak-case, at the temperature and pressure conditions (43 °C and 20 MPa) where the CO_2 enters the leakage pathway in the cement at 2000 m depth, the Joule-Thomson coefficient of CO_2 is 0.59 K/MPa; at the temperature and pressure conditions of the leakage pathway at 1500 m depth (33 °C and 15 MPa) the Joule-Thompson coefficient is 0.71 K/MPa. The temperature deviation from Ref-case at the thief zone Thz1 after 10, 30 and 50 days of leakage is about 1 °C, 1.6 °C and 2 °C. We note that only about 0.3 °C of this cooling is due to Joule-Thomson effect with the rest due to thermal conduction and convection from the leaking CO_2.

Once temperature anomalies are detected, it is helpful to examine the temperature history at individual locations, especially locations where the temperature anomalies are observed. While DTS measurements are continuous along the fiber, we use the term “DTS measurement location” to indicate discrete spatial locations that correspond to those elements in the numerical mesh that are used for the analysis. We plot the temperature change ΔT (the temperature difference between the current temperature T and temperature at day 0 before CO_2 injection, T_{0d}, i.e., $\Delta T = T - T_{0d}$) history at three selected locations (vertical elevation shown in Fig. 2) in Fig. 3, as well as the temperature change during the warm-up period relative to the temperature at the end of the injection (i.e., $\Delta T = T - T_{110d}$) in Fig. 4:

• Location 1: LB – the lowest DTS measurement location, “B” indicating the bottom point anomaly;

• Location 2: LM – the lowest DTS measurement location in the thief zone, i.e., where the leaking CO_2 starts to enter Thz1, “M” indicating a middle point anomaly;

• Location 3: LT – the DTS measurement location below the elevation where the leakage flow pathway ends, “T” indicating the top point anomaly.

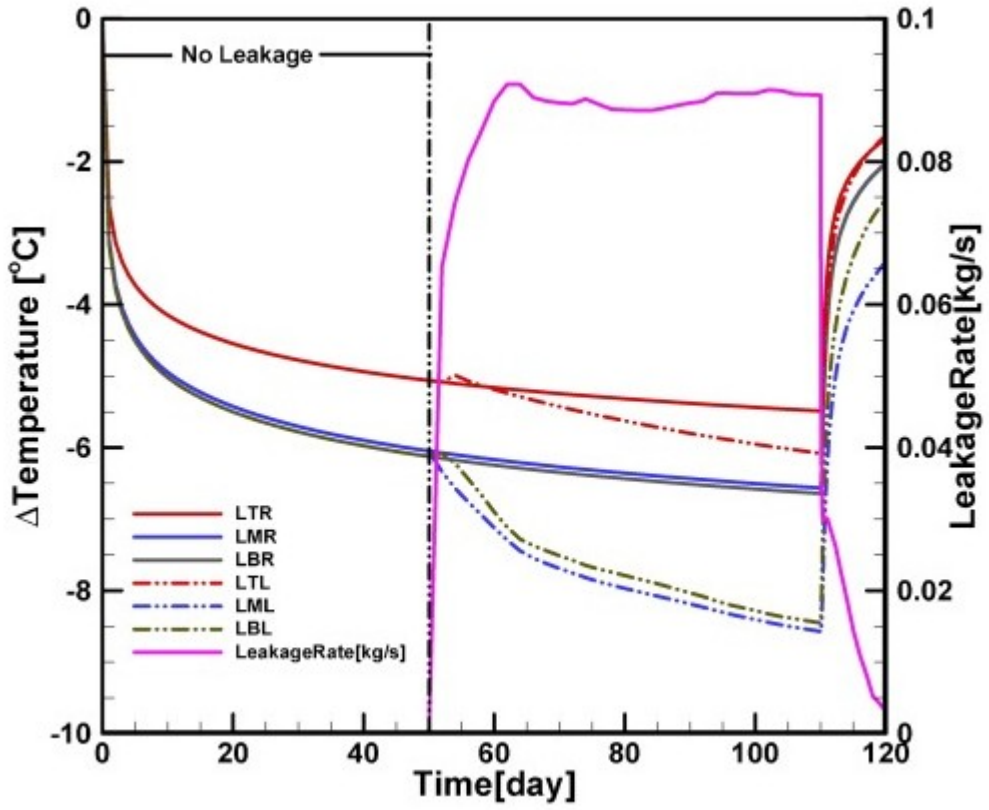

Fig. 3. The first Y axis shows the temperature change history at four DTS measurement locations for both Ref-case (notations end with "R") and Leak-case (notations end with "L"). LB – the lowest DTS measurement location in the numerical mesh; LM – the lowest DTS measurement location in the thief zone; LT – the DTS location right below the elevation where leakage pathway ends. The second Y axis shows the leakage flow rate for the Leak-case.

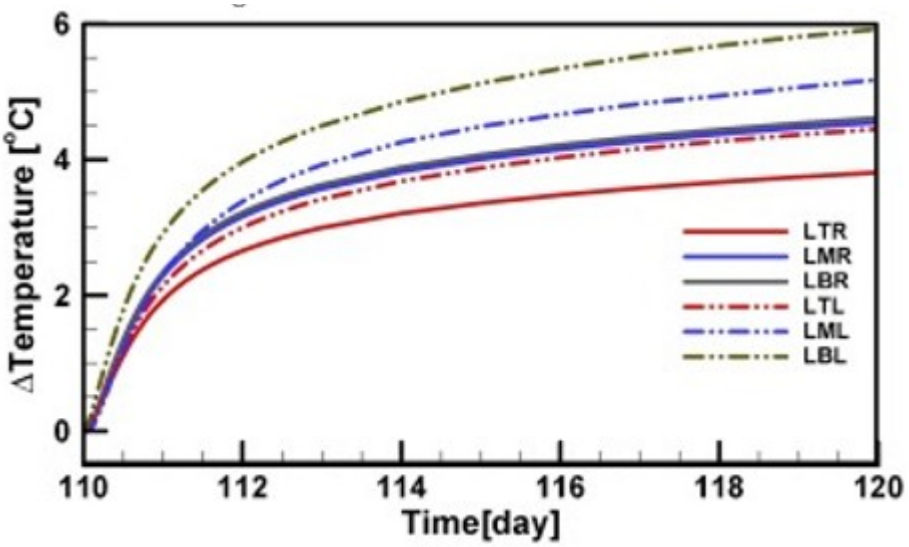

Fig. 4. Plot of ΔTemperature = Temperature – Temperature@110d for the warm-up period in Fig. 3.

The following observations are made from Fig. 3, Fig. 4: (1) For Ref-case, all three temperature curves are monotonically decreasing during CO_2 injection,

whereby the temperature decreases more rapidly during the initial phase due to the initial large temperature contrast between the injected fluid and formation; (2) for Leak-case, a distinct discontinuity appears in all three curves during injection, indicating leakage; (3) both the cooling during initial CO_2 injection before the temperature reaches quasi-steady state, and the warm-up after CO_2 injection stops are more pronounced at deeper than shallower locations because deeper locations are warmer before CO_2 leakage and the leaked CO_2 is coldest at the deepest leakage point, warming up as it ascends; and (4) the temperature increase after CO_2 injection stops is higher for Leak-case than for Ref-case as the stronger temperature gradient leads to higher conductive heat transfer through the casing. These observations provide us a roadmap for identifying leakage signals.

4.2. Minimum detectable leakage rate

To investigate the minimum detectable leakage rate, a set of simulations is performed to relate the leakage rate to the temperature changes observed by the DTS. In this section the temperature change ΔT is defined as the difference between the temperature measured at the time when leakage starts (at 50 day) and after 60 days of leakage (at 110 day), i.e., $\Delta T = T_{110d} - T_{50d}$. We examine the temperature change at three locations identified previously: (1) LB, the lowest elevation where DTS measurements are made; (2) LM, where the leaking CO_2 enters the thief zone; and (3) LT, where the leakage pathway ends.

Fig. 5 shows ΔT at these three locations for different leakage rates, assuming perfect knowledge of hydrogeological parameters (i.e., no parameter uncertainty). If there is no leakage (i.e., the reference case), ΔT at all three locations is about 0.5 °C, which reflects the transient, but near-steady cooling of the formation from the cold well. If the leakage rate is more than 0.002 kg/s, a larger ΔT can be observed at location LM. The other two locations show an increased ΔT only if the leakage rate exceeds about 0.05 kg/s. If no conceptual or parametric uncertainties are assumed, and the accuracy of DTS measurements is taken to be 0.1 °C, a leakage flow rate of 0.005 kg/s can be considered the minimum detectable leakage rate for this scenario. In reality, there are likely to be considerable modeling uncertainties and errors. Even assuming perfect knowledge of geological parameters, a minimum detectable leakage rate of 0.05 kg/s (corresponding to a temperature change greater than 1.0 °C) is considered more realistic if modeling errors are taken into account.

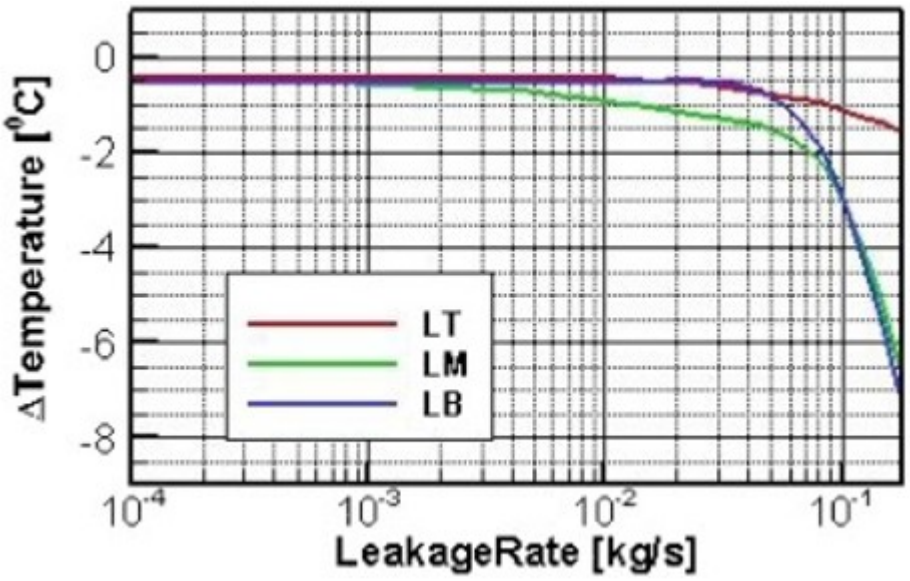

Fig. 5. ΔTemperature = $T_{110d} - T_{50d}$ at three locations as a function of leakage rate.

4.3. Effect of assumptions

In this section we consider the effects on leakage detection due to: 1. the leakage start time relative to the start of CO_2 injection; 2. the uncertainty in geological properties by simulating scenarios with different zone permeabilities; and 3. assumptions on where the leakage pathway ends.

1 The first assumption is that CO_2 leakage happens after a period of CO_2 injection without any leakage, i.e., temperature profiles representing near-steady state conditions can be used as a baseline for temperature anomaly detection. Such a reference profile may not be available if the well leaks immediately after injection commences due to a flaw in well construction. To understand if this assumption would affect the results, a simulation (Leak-case) is performed in which CO_2 starts leaking immediately after the well begins operation. The simulation includes 60 days of injection, followed by 3 days of warm up after injection stops. A simulation for Ref-case with the same operation is also performed. Fig. 6 shows the temperature evolution for these two cases. Three distinct anomalies similar to those observed for Leak-case in the base-case scenario indicate potential leakage. This suggests that a period of injection without CO_2 leakage is not a requirement for leakage detection. The reason for a period of injection without leakage is to avoid the situation in which uncertain thermal properties have an impact on the calculated temperature distribution before leakage starts. The duration of CO_2 injection before leakage occurs (e.g., 50 days in the base case scenario) does affect formation temperature adjacent to the well; however, this effect is relatively small. Moreover, it results in an approximately constant offset in the temperature profile, whereas leakage leads to localized temperature anomalies along the profile or in a time series, as discussed earlier. Reaching near-steady conditions prior to leakage initiation is thus not considered to be an important factor affecting leakage

detectability. Similarly, leakage of CO_2 may not happen suddenly. It could be a relatively slow process as the cement along the well casing degrades gradually. The temperature signal will become more pronounced as the leakage amount increases with increasing cement permeability over a long period of time.

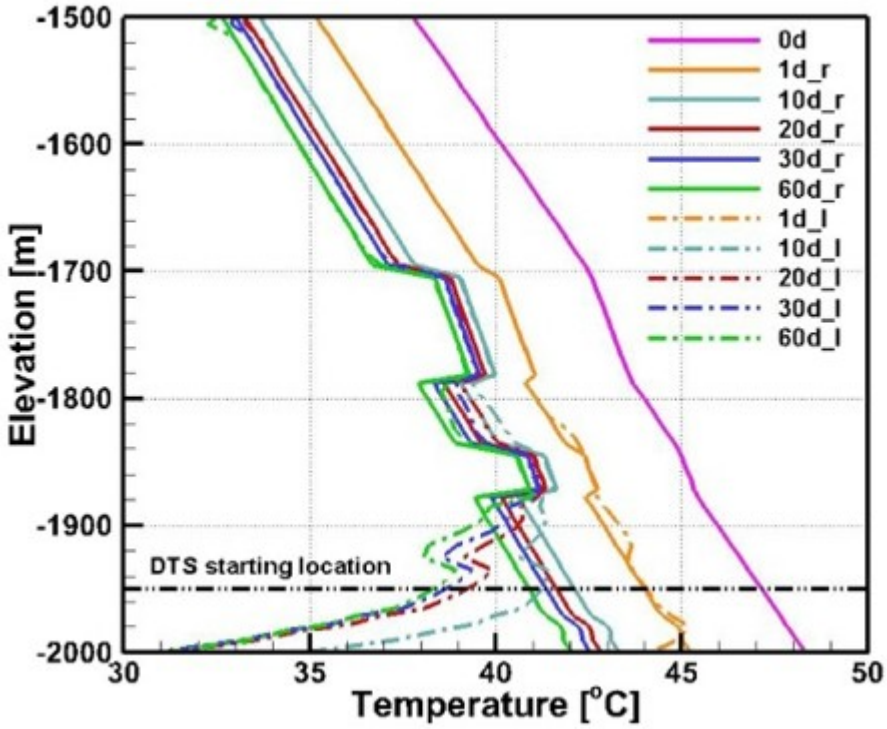

Fig. 6. Vertical temperature profiles for both Ref-case and Leak-case if the leakage started when the well begins operation.

2 The second assumption is that Thz1 is the lowest (or first) thief zone encountered by the leaking CO_2. The facts that Thz1 has a high permeability and it is located relatively deep, i.e., 110 m above the storage reservoir, are beneficial for leakage detection. Here, we explore two alternative possibilities considering large uncertainty in geological settings:

• There is no strong permeability contrast among geological layers, so the leaking CO_2never encounters a thief zone with a much higher permeability compared to other layers. The permeabilities of Thz1 and Thz2 are reduced from 1 D to 1 mD, this case is referred to as “Nothief”. The temperature changes as a function of leakage rate at the three locations LB, LM, and LT are shown in Fig. 7. Because no layer has a large permeability as a thief zone, the leaking CO_2 tends to migrate upwards along the casing until it reaches the top of the defect, where it accumulates, leading to a locally cold area. As a result, location LT develops a stronger temperature anomaly at a smaller leakage rate than the other two locations, and also than location LT in the base case (see Fig. 5).

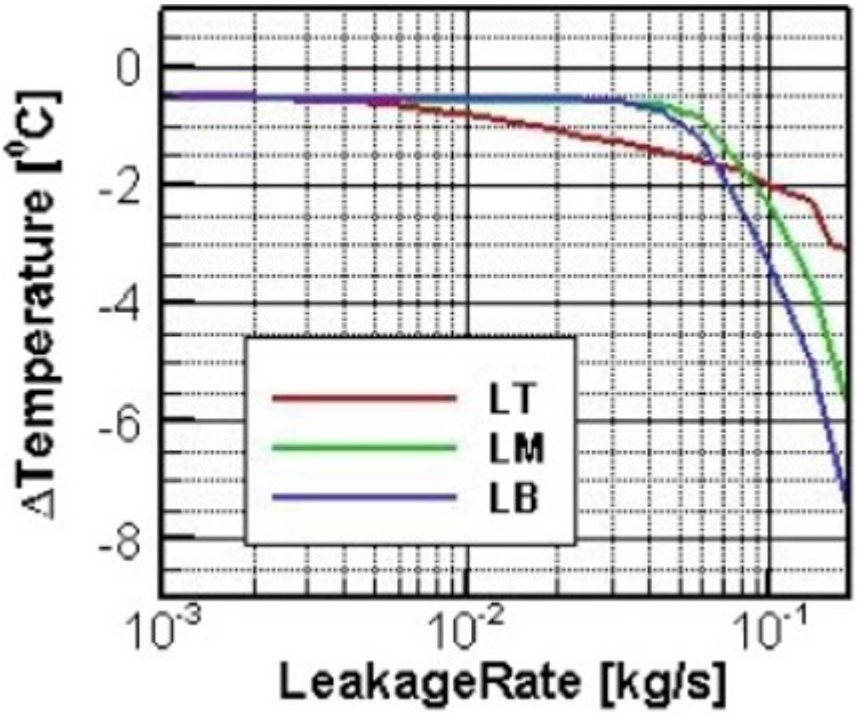

Fig. 7. Temperature change at three individual locations for case “Nothief”.

• The high-permeability zones are located at shallower depths (the permeability of Thz1 and Thz2 are reduced by three orders of magnitude, and the permeability of two sublayers within Thz3 (Thz32 and Thz34; locations shown in Fig. 8) are increased by three orders of magnitude, i.e., changed to 10^{-12} m^2), this case is referred to as “Thief_h”. The vertical temperature for this case is shown in Fig. 8. Because the high permeability zones are located at a much higher elevation, the temperature anomaly at the thief zone is not as strong as the base case. But a large deviation from Ref-case is still observed at the bottom DTS measurement location LB.

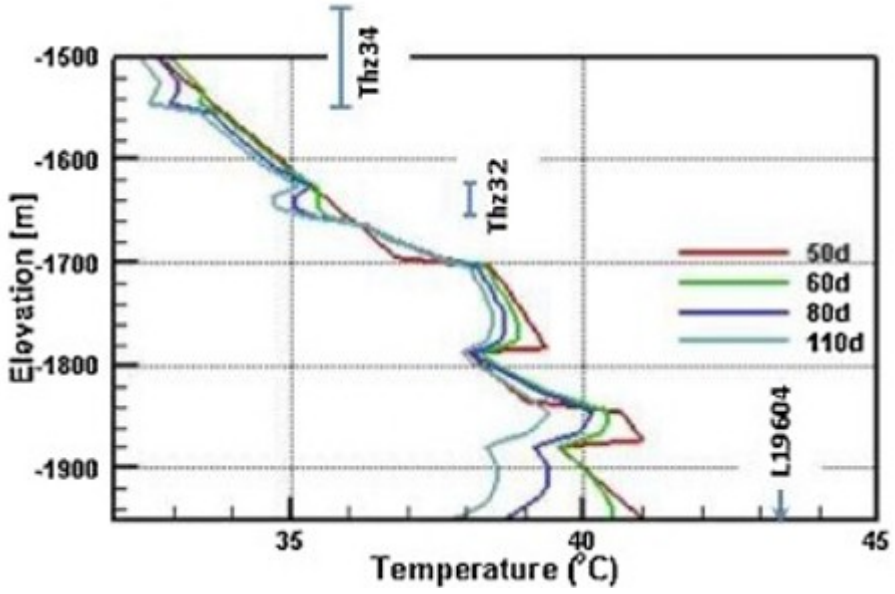

Fig. 8. Temperature development for “Thief_h” case, where the leakage pathway ends in the middle of a thief zone – zone Thz34. Thz32 is another thief zone.

In general, the thief zone location determines one of the anomaly locations. It has a minor impact on detecting anomalous temperature signals due to CO_2 leakage. The lower this thief zone is, the stronger the temperature anomaly is at that location, due to the stronger temperature contrast between the upflowing CO_2 and the formation in the lower part of the formation. The lack of a thief zone will enhance the anomaly where the leakage pathway ends.

1 The third assumption is that the leakage pathway along the casing ends at an elevation below ground surface at a trapping structure. If this were not the case, i.e., the CO_2 leakage pathway reaches the land surface, then there would not be CO_2accumulation due to structural trapping. In this case, leakage detection will mainly rely on anomalies at the other two locations, i.e., the lowest DTS measurement location and the location where CO_2 first enters a high-permeability thief zone. The temperature development at locations LB and LM will be similar to those in the base case scenario. If the leakage pathway ends in the middle of a thief zone as shown in Fig. 8, CO_2 may enter the thief zone and migrate upwards, and the temperature anomaly due to CO_2 intrusion will be mainly in the lower section of that thief zone, as shown in Fig. 8. Again, the lack of structural trapping may make it harder but does not prevent us from detecting CO_2 leakage along the well casing.

In addition to these explicit assumptions, an implicit assumption from the 2D model is that the degraded cement occupies the entire space around the well casing, forming a ring-shaped leakage pathway. In reality, the cement could be only locally degraded and be on the opposite side of the DTS cable, which will result in a less pronounced cooling signal due to leakage, and thus a higher leakage detectability threshold.

In summary, the base-case scenario used for the leakage detection analysis appears robust in that its assumptions do not significantly affect the ability of DTS measurements to detect leakage. If all the assumptions are satisfied, one expects at least three temperature anomalies indicating leakage. If no high-permeability thief zone exists, there will be no thief-zone-related temperature anomaly, but one may observe lower temperatures at the location where the leakage pathway ends. Similarly, if the leakage pathway goes all the way to the ground surface, or ends in the middle of a thief zone, one will rely on the other two anomalies. In rare occasions, where there is no thief zone, and leaking CO_2 is not structurally trapped, the lowest DTS measurement LB may be the only location available for leakage detection. In the next section, we will investigate the relationship between the temperature change at this location and the leakage rate to derive the minimum detectable leakage rate.

4.4. Effect of operational conditions

In the previous simulations a constant injection pressure was used. However, in reality, the operational conditions change frequently, and the injection pressure may not stay constant. To investigate this effect on leakage detection, in the course of simulation we add some pressure fluctuation at a few random times (see Fig. 9a). We make this pressure fluctuation more frequent around the leakage starting time (i.e., at 50 days). In addition, we add an injection pause between 51 and 52 days. Fig. 9b shows the vertical temperature profile at a few different times, both for the reference case and leakage case. The temperature at the depth of Thz1 is slightly higher for the leakage case at 51 days, due to the warm water being pushed up during the initial stage of leakage (e.g., water leakage rate is about 0.02 kg/s initially). This slightly higher temperature may by itself not be obvious enough for leakage detection. However, the non-smooth temperature profile at the thief zone indicates the possibility of leakage. This possibility can be confirmed later by the cooling trend at the lower end of the DTS, and the temperature depression at the thief zone when injection was resumed. By contrast, if there is no leakage, the entire temperature profile may be offset to lower or higher temperatures depending on the injection amount. We note that the temperature profiles at different times are more or less parallel to each other. Therefore, we conclude that the observed thermal anomalies are not significantly affected by operational conditions.

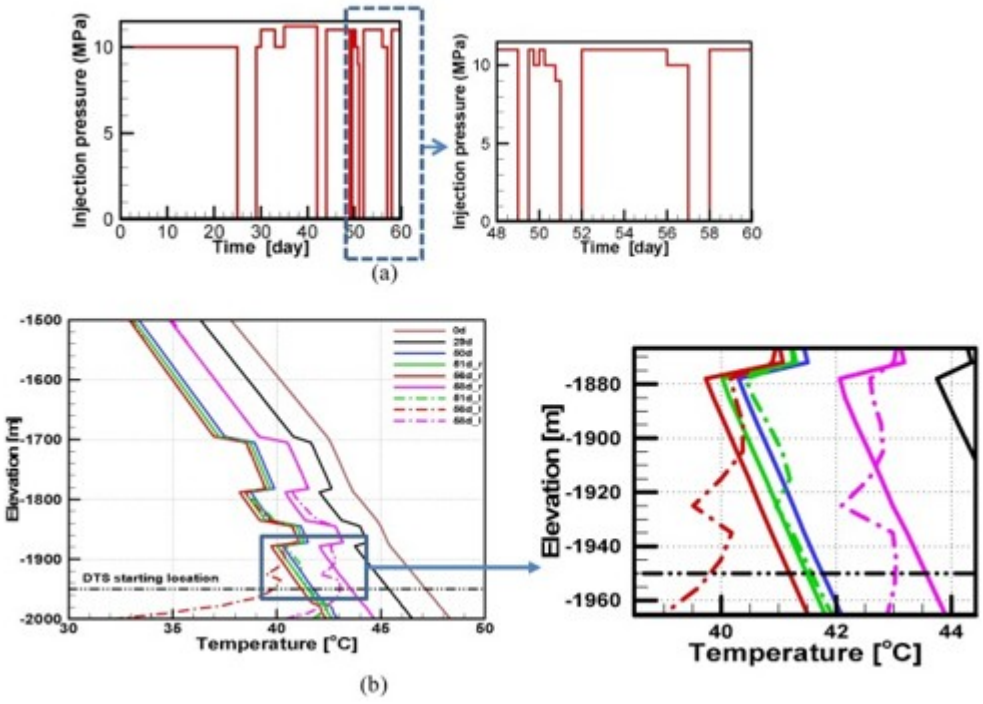

Fig. 9. (a). Injection pressure over time; (b). corresponding temperature profiles at the DTS location (leakage starts at 50 days). "_r" represent reference scenario (i.e., no leakage), showing in solid lines; "_l" represent the leakage scenario, showing in dashed-dotted lines. The two profiles are the same for the first 50 days.

4.5. Effect of injection temperature

In the simulation a constant injection temperature at 800 m is used. In reality, this temperature is most likely not constant, as it is affected by the operational conditions (injection rate, duration etc.) as well as CO_2 and formation temperature at ground surface, and geothermal gradient. The effect of changing injection temperature is similar to the effect of changing operational conditions. Specifically, when the injection temperature changes, the entire temperature profile may be offset to lower or higher temperatures, but the observed thermal anomalies are not significantly affected by the injected temperature.

4.6. Effects of uncertain parameters

The above discussion of the base-case scenario is contingent on the assumption that all hydraulic and thermal parameters are well known, except the permeability of the leakage pathway, which determines the leakage rate. However, in reality most properties listed in Table 2 are uncertain. In this section, we focus on how uncertainty affects the estimate of the minimum detectable leakage rate.

To explore the relationship between the leakage rate and temperature anomaly while accounting for parameter uncertainty, Monte Carlo (MC) simulations are performed using Latin hypercube sampling. Latin hypercube sampling is an efficient method to sample uncertain parameters based on their distributions, generating samples over the entire expected parameter range, with more samples taken in the region with higher probability. The uncertain parameters considered are: 1. permeability of the storage reservoir and all potential thief zones (Thz1, Thz2 and all sublayers in Thz3), assuming a lognormal distribution with a standard deviation of 0.25, with the mean at their respective base-case values (see Table 2); and 2. both wet and dry thermal conductivities, assuming a normal distribution with a standard deviation of 0.03 W/m °C for the inert material, a normal distribution with a standard deviation of 0.5 W/m °C for other materials listed in Table 2, and the means at the base-case values shown in Table 2. The thermal properties for the wellbore materials are well-known, so the standard deviations for those are small. There is much more variation in properties of the geological material. However, geological variability is mainly covered in the model by explicitly specifying discrete layers with very different properties.

The resulting temperature changes at LB as a function of leakage rate are shown as green symbols in Fig. 10. The change in leakage rate is an outcome of uncertain permeabilities. The red line is the temperature change at LB (from Fig. 5) without considering thermal parameter uncertainty. This plot not only shows the effect of uncertain parameters on the relationship between ΔT and different leakage rates, but also shows possibilities for potential false identification. The variation in ΔT could be between 0.5 and 1.0 °C simply due to uncertainty in the parameters, even though no leakage occurs. For example, a false positive leakage identification can be seen in Fig. 10, where a symbol at a (negligible) rate of 4.e–4 kg/s shows a large ΔT

of about 1.0 °C. On the other hand, Fig. 10 also shows that one of the leakage scenarios with a rate of approximately 0.05 kg/s yields a small ΔT of about 0.5 °C. If the parameters in this scenario were the actual values, one may conclude that there is no leakage; this would have resulted in a false negative leakage identification.

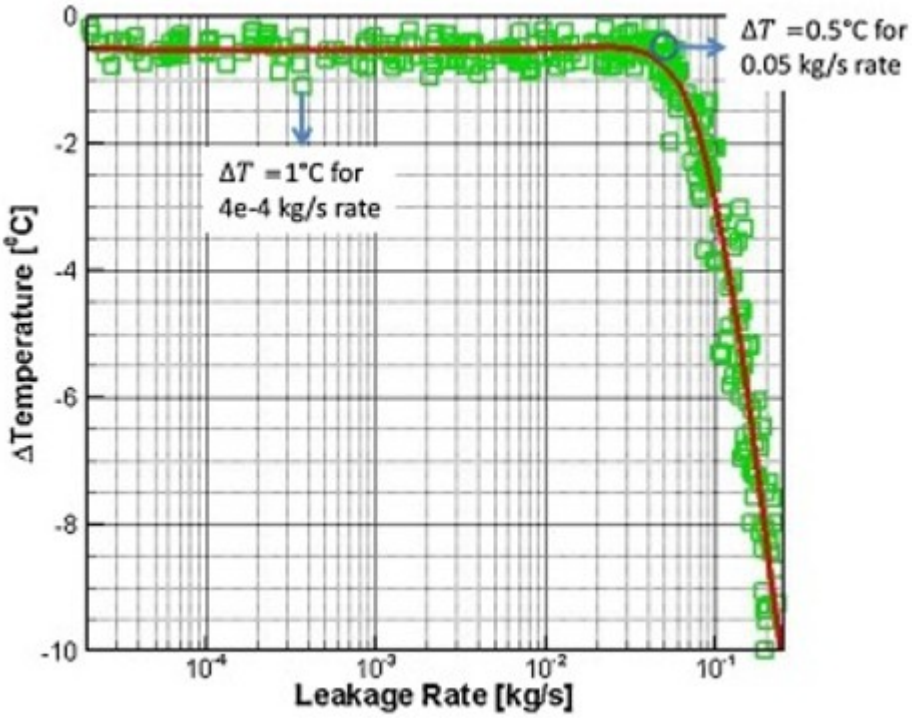

Fig. 10. CO_2 leakage rate vs. temperature change ΔT at the location LB. The red line is made assuming there is no uncertainty in all other parameters (except leakage flow rate), i.e., fixed parameters; the green symbols are made considering a number of uncertain parameters.

Based on the above discussion and potential modeling errors, we conclude that a minimum detectable leakage of about 0.1 kg/s is a reasonable estimate.

4.7. Discussion on potential false leakage identification

To investigate the potential of false identifications, a set of 100 realizations of thermal properties is generated, which vary according to their presumed uncertainty distributions described in the previous section. Three sets of Monte Carlo simulations are performed using these realizations: One set without CO_2 leakage (Set 1), one with the leakage rate approximately constant at 0.1 kg/s (Set 2), and one with the leakage rate around 0.05 kg/s (Set 3).

Results are presented as histograms of temperature changes ($\Delta T = T_{110d} - T_{50d}$) at location LB. Fig. 11(a) shows the comparison between the histograms of the no leakage set and 0.1 kg/s leakage rate set. There is no overlap between the two sets, suggesting that the chance of a false identification due to parameter uncertainty is very small when a minimum detectable leakage rate of 0.1 kg/s is used. However, Fig. 11(b) shows that

the histograms of the no leakage set and 0.05 kg/s leakage rate set overlap considerably, suggesting a large probability for false identification if a minimum leakage rate of 0.05 kg/s were used.

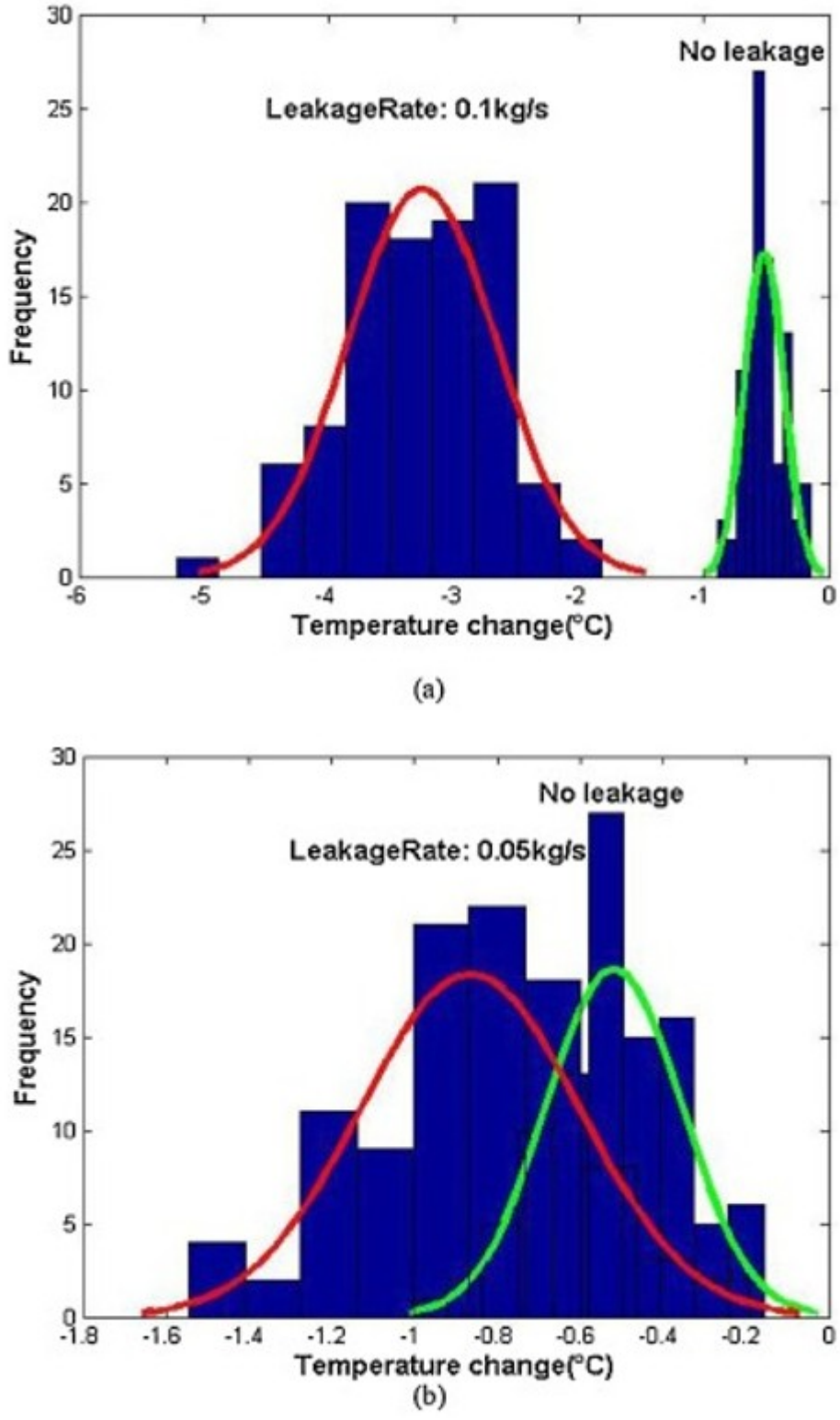

Fig. 11. Histogram of temperature change for the location LB, (a) no leakage case (the green curve on the right) vs. 0.1 kg/s leakage rate case (the red curve on the left); (b) no leakage case (the green curve on the right) vs. 0.05 kg/s leakage rate case (the red curve on the left).

In this section, we have investigated a few key factors for leakage detection, which include:

• Leakage rate (mainly controlled by leakage-pathway permeability)

• Uncertainty in the geological structures and geological parameters

• Thermal conductivities of the well materials and geological formations

This analysis considers a minimum detectable leakage rate of 0.1 kg/s appropriate when accounting for uncertainty in the parameters. For this conclusion to hold, the actual parameters should fall into the specified uncertainty ranges assumed in this study. Violations may, but do not necessarily, lead to false leakage identification. For example, the inert material between the steel tubing and the casing has a much smaller thermal conductivity (0.1 W/m °C) than other materials inside the wellbore, which makes it the most important thermal property in the analysis. If it were significantly outside the specified range, the conclusion may need to be modified accordingly.

5. Conclusions and summary

In summary, we applied numerical simulations to (1) investigate methods for identifying CO_2leakage along the well casing using DTS, and (2) for estimating the minimum detectable leakage rate. The main conclusions are as follows:

• The entire vertical temperature profile should be analyzed. Sudden changes in the profile may indicate the location of thief zones for leaked CO_2. Numerical simulations are needed to interpret the temperature measurements.

• At least one of three anomalies is expected if leakage along the well casing occurs: (1) The top of the CO_2 storage reservoir (or the lowest DTS measurement location) shows a relatively large temperature anomaly, because the temperature contrast is largest at this point, where the CO_2 is coldest (inside the leakage pathway) and the cement is warmest; (2) at the location where CO_2 first enters a high-permeability thief zone, as CO_2 accumulates in that zone; and (3) at the location where the leakage pathway in the cement ends, where CO_2 is trapped and may accumulate.

• Temperature history plots for locations with anomalies should be made. Discontinuities in these temperature history plots may indicate leakage.

• The post-injection warm-up period should be examined to confirm potential leakage.

• Simulations for estimating the minimum detectable leakage rate should be based on field conditions. Uncertainty in the parameters and geological structures will have an impact on the conclusions. Histograms obtained from Monte Carlo simulations considering uncertainty in thermal properties can be used to investigate the possibility for false identification. The probability of

false identification is given by the overlap area of the histograms calculated with and without leakage.

• For the case considered, the minimum detectable leakage rate is estimated to be 0.1 kg/s. This conclusion is established based on the uncertainty range specified in the study, the field conditions (e.g., depth) and the contrast between the injected fluid temperature and reservoir and formation temperature. If the actual parameters fall outside the specified range, the analysis should be modified based on the new uncertainty range.

Acknowledgmentss

The authors thank the two anonymous reviewers for their detailed review comments. We also wish to acknowledge the review provided by Christine Doughty of Lawrence Berkeley National Laboratory for her most useful suggestions. Funding to support this study has been provided by the Assistant Secretary of the Office of Fossil Energy, U.S. Department of Energy, National Energy Technology Laboratory under contract DE-AC02-05CH11231 and through the National Risk Assessment Partnership (NRAP) project.

References

Altunin, 1975

V.V. Altunin**Thermophysical Properties of Carbon Dioxide**

Publishing House of Standards, Moscow (1975)

(in Russian)

Bachu and Celia, 2009

S. Bachu, M. Celia**Assessing the potential for CO_2 leakage, particularly through wells, from CO_2 storage sites**

The Science and Technology of Carbon Sequestration, Vol. 183 (2009), pp. 203-216

Benson, 2006

S. Benson**Assessment of Risks from Storage of Carbon Dioxide in Deep Underground Geological Formations**

(2006)

http://www.uscsc.org/Files/Admin/Educational_Papers/AttachmentToUSCSCReportOnCCSSafetyPaper_GeologicalStorageRiskAssessment.pdf

Carey et al., 2010

J.W. Carey, R. Svec, R. Grigg, J. Zhang, W. Crow**Experimental investigation of wellbore integrity and CO_2–brine flow along the casing–cement microannulus**

Int. J. Greenhouse Gas Control, 4 (2) (2010), pp. 272-282

Celia et al., 2011

M. Celia, J.M.B. Nordbotten, M. Court Dobossy, S. Bachu**Field-scale application of a semi-analytical model for estimation of CO_2 and brine leakage along old wells**

Int. J. Greenhouse Gas Control (2011), p. 5, 10.1016/j.ijggc.2010.10.005

Crow et al., 2010

W. Crow, J.W. Carey, S.E. Gasda, D.B. Williams, M.A. Celia**Wellbore integrity of natural CO_2 producer**

Intl. J. Greenhouse Gas Control, 4 (2010), pp. 186-197

Doughty and Freifeld, 2013

C. Doughty, B.M. Freifeld**Modeling CO_2 injection at Cranfield, Mississippi: investigation of methane and temperature effects**

Greenhouse Gas Sci. Technol., 3 (2013), pp. 475-490, 10.1002/ghg.1363

Duguid et al., 2011

A. Duguid, M. Radonjic, G.W. Scherer**Degradation of cement at the reservoir/cement interface from exposure to carbonated brine**

Int. J. Greenhouse Gas Control, 5 (6) (2011), pp. 1413-1428, 10.1016/j.ijggc.2011.06.007

Duguid et al., 2013

A. Duguid, R. Butsch, J.W. Carey, M. Celia, N. Chugunov, S. Gasda, T.S. Ramakrishnan, V.Stamp, J. Wang**Pre-injection baseline data collection to establish existing wellbore leakage properties**

Energy Procedia (2013), p. 37, 10.1016/j.egypro.2013.06.488

Finsterle et al., 2008

S. Finsterle, C. Doughty, M.B. Kowalsky, G.J. Moridis, L. Pan, T. Xu, Y. Zhang, K. Pruess**Advanced vadose zone simulations using TOUGH**

Vadose Zone J., 7 (2008), pp. 601-609, 10.2136/vzj2007.0059

Finsterle, 2004

S. Finsterle**Multiphase inverse modeling: review and iTOUGH2 applications**

Vadose Zone J., 3 (2004), pp. 747-762

Garcia, 2003

J.E. Garcia**Fluid Dynamics of Carbon Dioxide Disposal into Saline Aquifers, PhD Dissertation**

University of Berkeley, Berkeley, California (2003)

Gasda et al., 2008

S.E. Gasda, J.M. Nordbotten, M.A. Celia**Determining effective wellbore permeability from a field pressure test: a numerical analysis of detection limits**

Environ. Geol., 54 (2008), pp. 1207-1215, 10.1007/s00254-007-0903-7

Gasda et al., 2013

S. Gasda, M. Celia, J. Wang, A. Duguid**Wellbore permeability estimates from vertical interference testing of existing wells**

Energy Procedia, 37 (2013), pp. 5673-5680

Henninges, 2010

J. Henninges**Permanent distribution temperature sensing at the Ketzin CO_2 storage test site**

IEAGHG 6th Wellbore Network Meeting (2010)

http://www.ieaghg.org/docs/General_Docs/6wellbore/Presentations/Day2/14.25Henninges.pdf

International Formulation Committee, 1967

International Formulation Committee (IFC)**A Formulation of the Thermodynamic Properties of Ordinary Water Substance**

IFC Secretariat, Düsseldorf, Germany (1967)

Kutchko et al., 2007

B. Kutchko, B. Strazisar, D. Dzombak, G. Lowry, N. Thaulow**Degradation of well cement by CO_2 under geologic sequestration conditions**

Environ. Sci. Technol., 41 (2007), pp. 4787-4792

Liebscher et al., 2013

A. Liebscher, F. Möller, A. Bannach, S. Köhler, J. Wiebach, C. Schmidt-Hattenberger, M.Weiner, C. Pretschner, K. Ebert, J. Zemke**Injection operation and operational pressure-temperature monitoring at the CO_2 storage pilot site Ketzin, Germany – design, results, recommendations**

Int. J. Greenhouse Gas Control, 15 (2013), pp. 163-173, 10.1016/j.ijggc.2013.02.019

Mao et al., 2017

Y. Mao, M. Zeidouni, R. Askari**Effect of leakage pathway flow properties on thermal signal associated with the leakage from CO_2storage zone**

Greenhouse Gases: Sci. Technol., 7 (2017), pp. 512-529

Núñez-López, 2011

V. Núñez-López**Temperature monitoring at SECARB Cranfield Phase 3 site using distributed temperature sensing (DTS) technology**

Poster Presented at the 10th Annual NETL Carbon Capture & Sequestration Conference, Pittsburgh, Pennsylvania, May 2–5, 2011. GCCC Digital Publication Series #11-10 (2011)

Nogues et al., 2011

J.P. Nogues, J.M. Nordbotten, M. Celia**Detecting leakage of brine or CO_2 through abandoned wells in a geological sequestration operation using pressure monitoring wells**

Energy Procedia, 4 (2011), pp. 3620-3627, 10.1016/j.egypro.2011.02.292

Nogues et al., 2012

J.P. Nogues, B. Court, M. Dobossy, J.M. Nordbotten, M.A. Celia**A methodology to estimate maximum probable leakage along old wells in a geological sequestration operation**

Int. J. Greenhouse Gas Control, 7 (2012), pp. 39-47, 10.1016/j.ijggc.2011.12.003

Nordbotten et al., 2005

J.M. Nordbotten, M. Celia, H. Dahle**Semi-analytical solution for CO_2 leakage through an abandoned well**

Environ. Sci. Technol., 39 (2) (2005), pp. 602-611, 10.1021/es035338i

Nordbotten et al., 2009

J.M. Nordbotten, D. Kavetski, M. Celia, S. Bachu**Model for CO_2 leakage including multiple geological layers and multiple leaky wells**

Environ. Sci. Technol., 43 (3) (2009), pp. 743-749, 10.1021/es801135v

Pan and Oldenburg, 2014

L. Pan, C.M. Oldenburg**T2Well—an integrated wellbore-reservoir simulator**

Comput. Geosci., 65 (2014), pp. 46-55, 10.1016/j.cageo.2013.06.005

Paterson et al., 2011

L. Paterson, C. Boreham, M. Bunch, J. Ennis-King, B. Freifeld, R. Haese, C. Jenkins, M.Raab, R. Singh, L. Stalker**The CO2CRC Otway Stage 2 B Residual Saturation and Dissolution Test: Test Concept, Implementation and Data Collected, Milestone Report to ANLEC**

(2011)

http://hub.globalccsinstitute.com/sites/default/files/sites/default/files/co2crc-otway-stage2b-residual-saturation-dissolution-test.pdf

Pruess and Spycher, 2007

K. Pruess, N. Spycher**ECO2N – a fluid property module for the TOUGH2 code for studies of CO_2 storage in saline aquifers**

Energy Convers. Manage. (2007), 10.1016/j.enconman.2007.01.016

Pruess et al., 2011

K. Pruess, C. Oldenburg, G. Moridis**TOUGH2 user's guide, version 2.0 (revised)**

Lawrence Berkeley Laboratory Report LBL-43134, Berkeley, California (2011)

http://esd.lbl.gov/FILES/research/projects/tough/documentation/TOUGH2_V2_Users_Guide.pdf

Pruess, 2008

K. Pruess**On CO_2 fluid flow and heat transfer behavior in the subsurface, following leakage from a geologic storage reservoir**

Environ. Geol., 54 (8) (2008), pp. 1677-1686

Watson and Bachu, 2009

T.L. Watson, S. Bachu**Evaluation of the potential for gas and CO_2 leakage along wellbores**

SPE, 106817 (2009), p. 7, 10.2118/106817-PA

Wiese, 2014

B. Wiese**Thermodynamics and heat transfer in a CO_2 injection well using distributed temperature sensing (DTS) and pressure data**

Int. J. Greenhouse Gas Control, 21 (2014), pp. 232-242, 10.1016/j.ijggc.2013.12.009

Zahasky and Benson, 2014

C. Zahasky, S.M. Benson**Evaluation of the effectiveness of injection termination and hydraulic controls for leakage containment**

Energy Procedia, 63 (2014), pp. 4666-4676, 10.1016/j.egypro.2014.11.500

GHGT-12

Zeidouni et al., 2014

M. Zeidouni, J.P. Nicot, S.D. Hovorka**Monitoring above-zone temperature variations associated with CO_2 and brine leakage from a storage aquifer**

Environ. Earth Sci., 72 (1733) (2014), 10.1007/s12665-014-3077-0

Zeng et al., 2012

F.H. Zeng, G. Zhao, L.J. Zhu**Detecting CO_2 leakage in vertical wellbore through temperature logging**

Fuel, 94 (2012), pp. 374-385

Zhang and Bachu, 2011

M. Zhang, S. Bachu**Review of integrity of existing wells in relation to CO_2 geological storage: what do we know?**

Int. J. Greenhouse Gas Control, 5 (2011), pp. 826-840, 10.1016/j.ijggc.2010.11.006

Zhang et al., 2010

Y. Zhang, C.M. Oldenburg, S. Finsterle**Percolation-theory and fuzzy rule-based probability estimation of fault leakage at geologic carbon sequestration sites**

Environ. Earth Sci., 59 (2010), pp. 1447-1459, 10.1007/s12665-009-0131-4

Zhang et al., 2011

Y. Zhang, B. Freifeld, S. Finsterle, M. Leahy, J. Ennis-King, L. Paterson, T. Dance**Single-well experimental design for studying residual trapping of supercritical carbon dioxide**

Int. J. Greenhouse Gas Control, 5 (2011), pp. 88-98, 10.1016/j.ijggc.2010.06.011